Metal Coordinated Tri- and Tetraborane Analogues

Sourav Kar, Subhash Bairagi, Ketaki Kar, Thierry Roisnel, Vincent Dorcet, Sundargopal Ghosh

10.1002/ejic.202100687

WILEY-VCH

Metal Coordinated Tri- and Tetraborane Analogues

Sourav Kar,[a] Subhash Bairagi,[a],§ Ketaki Kar,[a],§ Thierry Roisnel,[b] Vincent Dorcet,[b] and Sundargopal Ghosh*[a]

[a] Mr. S. Kar, Mr. S. Bairagi, Ms. K. Kar, Prof. Dr. S. Ghosh
Department of Chemistry
Indian Institute of Technology Madras
Chennai 600036, India. Tel: +91 44-22574230
E-mail: sghosh@iitm.ac.in, URL: http://chem.iitm.ac.in/Faculty/ghosh/
[b] Dr. T. Roisnel, Dr. V. Dorcet
ISCR (Institut des Sciences Chimiques de Rennes)
Univ Rennes, CNRS
UMR 6226, F-35000 Rennes, France
§ S. B. and K. K. are equal second authors.

Supporting information for this article is given via a link at the end of the document

Abstract: A series of triborane and tetraborane analogues have been isolated and structurally characterized utilizing chalcogenatoborate ligands Li[BH_3(EPh)] (E = S or Se). Thermolysis of [Cp*$TaCl_4$] in the presence of Li[BH_3(SPh)] afforded bimetallic tantallaheteroborane [(Cp*Ta)$_2$(μ-η^3:η^3-B_2H_4S)(μ-η^2:η^2-SBH_3)] (**1**) and hexasulfido trimetallic complex [(Cp*Ta)$_3$(μ-S)$_4$(μ-SPh)$_2$] (**2**). Compound **1** is a fused ditantallaheteroborane, in which both di- and triborane analogues are stabilized by two tantalum atoms. In an attempt to synthesize the selenium analogues of **1** and **2**, room-temperature reaction of [Cp*$TaCl_4$] with Li[BH_3(SePh)] was carried out, which afforded bimetallic tantallaheteroborane [(Cp*Ta)$_2${μ-η^3:η^3-B_3H_6(SePh)}{μ-SePh}$_2$] (**3**), monometallic tantallaheteroboranes [Cp*Ta(SePh)$_2${B_4H_{8-n}(SePh)$_n$}] (**4**: n = 0, **5**: n = 1), and trimetallic species [(Cp*Ta)$_3$(μ-Se)$_4${μ-Se_2(Se)}] (**6**). Compound **3** is the rarest example of triborane analogue {B_3H_6(SePh)} in the coordination sphere of two tantalum atoms. Whereas compounds **4** and **5** are examples of unsaturated metallaheteroboranes, in which the tetraborane analogues are stabilized in the coordination sphere of tantalum. One of the unique features of **3** and **5** is the presence of terminal B-SePh. Compound **6** has similar Ta_3Se_6 trisbutterfly core as that of **2** with additional bridging selenide unit. All the compounds have been characterized by NMR spectroscopy, mass spectrometry, IR spectroscopy and single-crystal X-ray diffraction studies.

Introduction

Lower boranes, such as diborane, triborane, and tetraborane are very special because of their unique bonding, abnormal structure, and unusual reactivities.[1,2] Some of them have significantly been employed in many organic syntheses, such as, catalytic diboration and borylation reactions.[1b-c,2] Most of the triboranes and tetraboranes are typically isolated in ring form.[1a] Interestingly, the chain forms of them are not very usual as with the increase of boron atoms they tend to form clusters.[3] However, utilizing transition metal templates these smaller boranes have been isolated both in chain and ring forms (Scheme 1).[4-9] In this connection, one suitable approach was developed by Fehlner and co-workers[10] employing cyclopentadienyl metal chlorides and monoborane reagents that led to the isolation of metal(s) coordinated smaller borane molecules. For example, recently we have isolated a classical [B_2H_5]$^-$ species in the coordination sphere of tantalum template.[9a] Likewise, the triborane species **I** and **II** were stabilized in the coordination spheres of dicobalt and dimolybdenum, respectively.[4,5c] The tetraborane **IV**, shown in Scheme 1, is stabilized at dichromium template.[6a-c] Recently, Braunschweig, Marder, and co-workers have isolated a tetraborane species **V** which is stabilized at diruthenium template.[8a] Apart from distinctive structural and bonding features, these metallaboranes, comprising of lower boranes, have a wide range of applications in catalysis, cyclotrimerization, borylation, etc.[11]

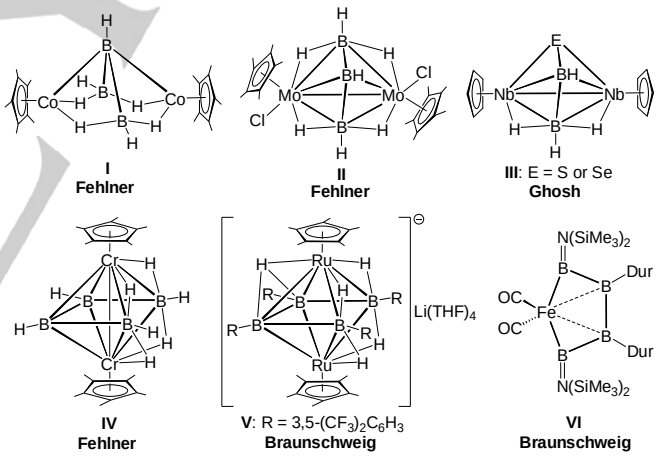

Scheme 1. Various types of metal-coordinated tri- and tetraboranes (For clarity, two μ-EPh units attached to Nb-Nb bond are omitted in **III**; **VI**: Dur = 2,3,5,6-tetramethylphenyl).

However, the development in this field found out to be very slow due to lack of alternative synthetic strategy and thus, search for an alternative synthetic strategy became essential. Interestingly, the progress in this field was significantly enhanced by the discovery of isolobal analogy[12] and electron-counting rules[13-15] that provided the basis for understanding the interrelationships among structures and compositions. Indeed, the replacement of one/two boron atoms of these smaller boranes with chalcogen atoms led to the stabilization of these species.[16,17] For example, we have recently explored the reactivity of Li[BH_3(EPh)] (E = S or Se) with [Cp_2VCl_2] that yielded chalcogen included divanadaboranes having similar

structural features with that of $[B_2H_6]$ complexes.[16] On the other hand, treatment of $Li[BH_3(EPh)]$ (E = S or Se) with $[CpNbCl_4]$ yielded chalcogen incorporated triborane analogue **III**.[16] As a result, with an objective of isolating triborane and tetraborane analogues, we have explored the chemistry of $[Cp^*TaCl_4]$ with chalcogen containing ligands, $Li[BH_3(EPh)]$ (E = S or Se) under diverse reaction conditions. Herein, in this article, we report the synthesis and characterization of several tantallaheteroboranes, which are analogues of triborane and tetraborane species.

Results and Discussion

Reactivity of $[Cp^*TaCl_4]$ with $Li[BH_3(EPh)]$ (E = S or Se).

In an attempt to synthesis smaller boranes in the coordination sphere of tantalum, the reaction of $[Cp^*TaCl_4]$ with four equivalents of $Li[BH_3(SPh)]$ was carried out at elevated conditions. The reaction afforded fused ditantallaheteroborane **1** (9% yield, R_f = 0.89) and fused trimetallic hexa-sulfido complex **2** (10% yield, R_f = 0.62) (Scheme 2). When the reaction was carried out with $Li[BH_3(SePh)]$ at room-temperature, it yielded ditantallaheteroborane **3** (12% yield, R_f = 0.28), monometallic tantallaheteroboranes **4** (20% yield, R_f = 0.34) and **5** (8% yield, R_f = 0.32), and fused trimetallic heptaselenido complex **6** (10% yield, R_f = 0.24) (Scheme 2). The formation of these metallaheteroboranes and chalcogen-ligated metal complexes is the concurrence of several reactions in one pot that vary from the binding of the anionic ligands, salt elimination, B–B formation, BH_3–EPh cleavage, etc. The detailed characterizations of these molecules are described below.

Ditantallaheteroborane 1. Compound **1** was isolated as yellow solid in 9% yield. The $^{11}B\{^1H\}$ NMR of **1** exhibits three resonances, appeared at δ = 31.8, -12.0, and -22.6 ppm with equal intensity. The peaks in the negative region indicate boron attached to electronegative sulfur atom. The resonance at δ = 2.09 ppm in the ^1H NMR spectrum suggests the existence of one kind of Cp* environment. Further, the ^1H NMR spectrum of **1** displays peaks at δ = -7.99 and -10.19 ppm, which indicate the presence of bridging Ta-H-B protons. The mass spectrum of **1** displays a molecular ion peak at *m/z* 753.1644 $[(M\text{-}H) + NH_4]^+$. All these spectroscopic data were not enough to reveal the structure of **1**. As a result, we have carried out a single-crystal X-ray analysis on a suitable crystal of compound **1**.

The solid-state X-ray structure of **1**, shown in Figure S1, evidently shows the core geometry as an edge-fused tantallaheteroborane $[(Cp^*Ta)_2(\mu\text{-}\eta^3\text{:}\eta^3\text{-}B_2H_4S)(\mu\text{-}\eta^2\text{:}\eta^2\text{-}SBH_3)]$. The spectroscopic data nicely corroborate with the solid-state structure of **1**. For example, the $^{11}B\{^1H\}$ chemical shifts of **1** for the sulfur-connected boron atoms appeared in the upfield region. The $^{11}B\{^1H\}$ resonances of **1** at δ = 31.8, -12.0, and -22.6 ppm are assigned to B1, B2, and B3, respectively, by means of calculated ^{11}B NMR.[18] The Ta-Ta bond distance of 2.763(6) Å in **1** is significantly shorter as compared to the Ta-Ta bond distances of $[(TaCp^*)_3(\mu_3\text{-}S)_3(\mu\text{-}S)_3B(SH)]$[19] (*c.a.* 3.106 Å) and $[(TaCp^*)_2(\mu\text{-}H)(B_2H_5)(SCH_2S)_2]$[9a] (3.2903(8) Å). However, it is comparable with those of $[(TaCp^*)_2(\mu\text{-}Se)\{B_3H_6(SePh)\}]$[16] (2.815(1) Å) and $[(Cp^*TaBr)_2(B_2H_6)]$[20] (2.83 Å). Further, the WBI[21] value of 0.85 for Ta-Ta bond along with the contour line diagram[22] of Laplacian of electron density of **1** support a strong Ta-Ta bonding interaction (Figure 1b). As shown in Figure S1, the geometry of **1** can be considered as the fusion of two clusters, trigonal bipyramidal $\{Ta_2B_2S\}$ and tetrahedron $\{Ta_2BS\}$. The $\{Ta_2B_2S\}$ fragment of cluster **1** has trigonal bipyramidal geometry, which is structurally identical to $[\{NbCp(EPh)\}_2\{B_2H_4E\}]$[16] (E = S or Se) and $[(Cp^*MoCl)_2B_3H_7]$.[4] The other part of cluster **1**, i.e., tetrahedron $\{Ta_2BS\}$, has similar structural features as that of diborane(6) species in bimetallic template. Therefore, compound **1** can also be viewed as a fused cluster where the triborane analogue and diborane analogue are stabilized in a ditantalum coordination sphere.

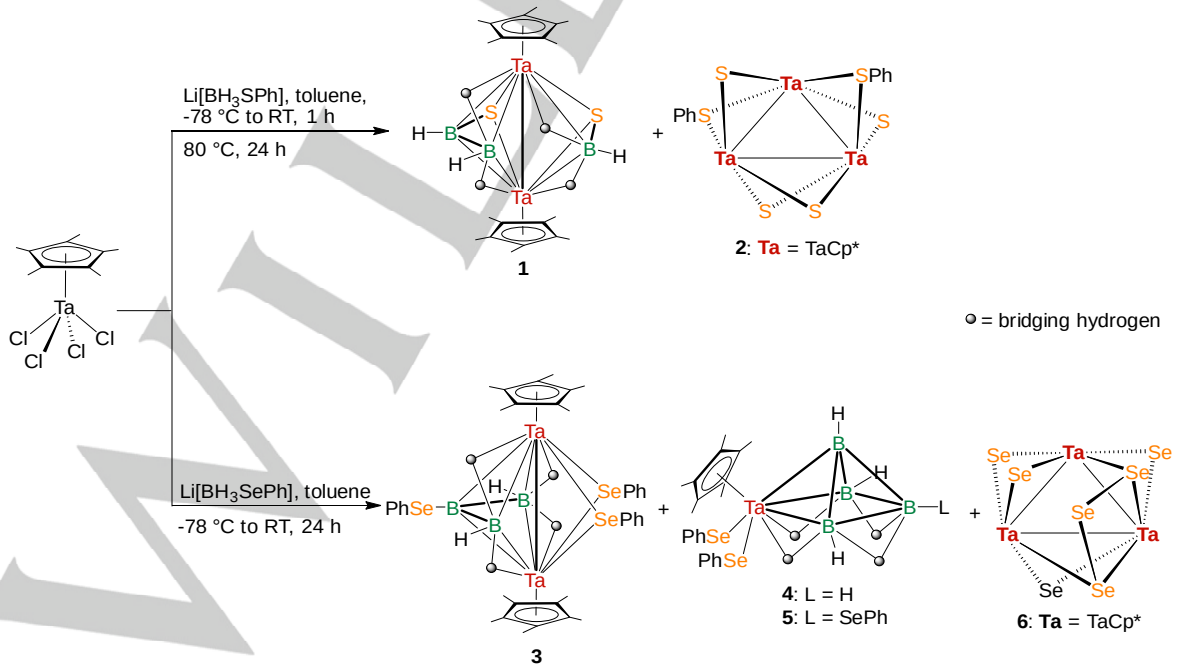

Scheme 2. Syntheses of ditantallaheteroboranes (**1** and **3**), tantallaheteroboranes (**4** and **5**) and trimetallic polychalcogenide complexes (**2** and **6**).

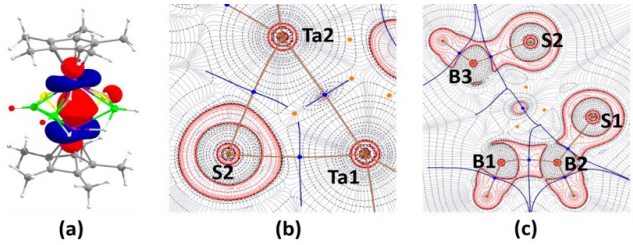

Figure 1. (a) HOMO-1 of **1** depicts Ta-Ta bonding interaction; (b) and (c) Contour line diagrams of the Laplacian of electron density along the Ta1–S2-Ta2 and a plane perpendicular to Ta1–Ta2 bond planes of **1**, respectively.

Triborane analogue 3. Compound **3** was isolated as purple solid in 12% yield. The $^{11}B\{^{1}H\}$ NMR spectrum of **3** shows three equivalents chemical shifts at δ = 24.5, 17.2, and 11.3 ppm. The ^{1}H chemical shift at δ = 2.20 ppm suggests the existence of one kind of Cp* protons, which is further confirmed by $^{13}C\{^{1}H\}$ NMR. Further, the ^{1}H NMR spectrum shows peaks at δ = -7.00 and -7.76 ppm with a ratio of 2:2 that indicates the existence of four Ta-H-B bridging protons. The $^{1}H\{^{11}B\}$ NMR spectrum shows peaks at δ = 6.38 and 6.07 ppm with a 1:1 ratio, which may be due to the terminal B-H protons. The mass spectrum of **3** displays a molecular ion peak at *m/z* 1140.0769 $[M]^+$. All these spectroscopic data were not adequate to predict the identity of **3** until a single-crystal X-ray diffraction analysis was carried out.

The solid-state X-ray structure of **3** displays a bimetallic metallaheteroborane $[(TaCp^*)_2\{\mu\text{-}\eta^3\text{:}\eta^3\text{-}B_3H_6(SePh)\}\{\mu\text{-}SePh\}_2]$ (Figure 2). The geometry of **3** is trigonal bipyramidal, in which one of the boron atoms and two tantalum atoms are in the equatorial positions, whereas the other two boron atoms are in the axial positions. The Ta-Ta bond is bridged by two {SePh} ligands and is slightly longer (2.7917(4) Å) than that of **1**. Further, the contour line map along the Ta1-Ta2-Se2 plane of **3** presents BCP and the bond path between Ta centers (Figure S27). The WBI of 0.83 between the Ta centers of **3** additionally supports the presence of strong Ta-Ta bonding interaction. The tantalum centers of **3** are at +4 oxidation state. On the other hand, the *av.* B-B bond distance of **3** (1.66 Å) is somewhat shorter than the B-B bond distances in other metallaboranes and metallaheteroboranes.[9a,16] In order to assign the boron atoms, we have calculated ^{11}B NMR chemical shifts for **3**. The calculated chemical shifts at δ = 17.7, 12.2, and 7.8 ppm correspond to B2, B3, and B1, respectively, that corroborate with the experimental $^{11}B\{^{1}H\}$ NMR with an error range of 3.5-7 ppm. One of the key features of **3** is the activation of one of the B-H bonds and the formation of the B-Se bond.

Besides the existence of B_3H_8-metal complexes, the number of structurally characterized triboranes at the coordination sphere of metals is very limited.[4,5] Compound **3** can be viewed as the triborane analogue stabilized in the coordination sphere of two tantalum atoms and is one of the potential entries to the limited series of transition metal coordinated triboranes. The $[Ta_2B_3]$ core of **3** possesses trigonal bipyramidal geometry, which is geometrically identical to that of electronically unsaturated transition metal coordinated triborane species $[(Cp^*MoCl)_2B_3H_7]$.[4] Although several M_2B_3 cores are known with open geometry, to the best of our knowledge **3** is the second example with *closo*-geometry after $[(Cp^*MoCl)_2B_3H_7]$. According to Wade's skeleton electron counting rule,[13] the number of skeletal electron pairs (SEP) required for the trigonal bipyramid is six (CVE = 42). Compound **3** has six skeletal electron pairs (CVE = 42); thus, it is electronically saturated.

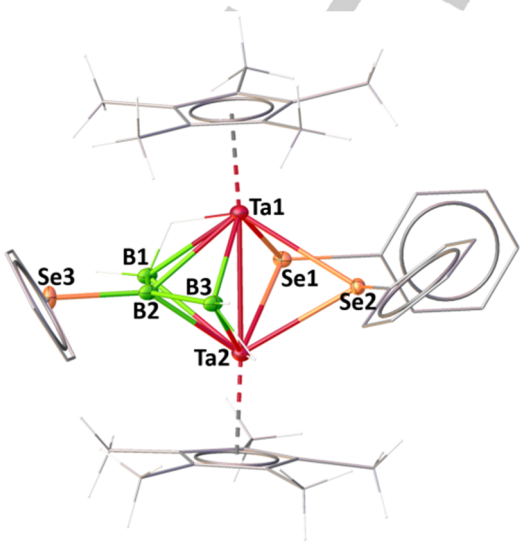

Figure 2. Molecular structure of **3**. Note that hydrogen atoms of phenyls are not shown for clarity. Selected bond lengths (Å) and angles (°) of **3**: Ta1-Ta2 2.7917(4), Ta1-B2 2.392(7), Ta1-B3 2.429(7), Ta2-B2 2.397(7), Ta2-B1 2.423(7), Ta2-Se2 2.7064(6), B1-B2 1.654(10), Se3-B2 2.024(7); Ta2-Se2-Ta1 62.012(15), Ta2-B1-Ta1 70.09(18), B1-B2-B3 132.5(6).

Electronic structure analyses of 1 and 3. As bimetallic **1** comprises of diborane and triborane analogues and bimetallic **3** consists triborane analogues, a theoretical investigation of their electronic structure and bonding became necessary. Computational analyses of **3** show a large HOMO-LUMO gap for **1** (3.509 eV) than that of **3** (3.037 eV). The HOMO-1 of both **1** (Figure 1b) and **3** (Figure 3b) depict the d orbital overlap of two Ta centers, which along with WBI and contour line diagram of Laplacian of electron density (Figures 1b and S27) support the strong Ta-Ta bonding in **1** and **3**. The contour map of **1** perpendicular to Ta1–Ta2 bond (Figure 1c) shows BCPs and the bond path between B1–B2 and B2–S1 (represent triborane analogue) and between B3–S2 (represent diborane analogue). The contour map of **3** along B1–B2–B3 plane represents BCPs and the bond path between all these boron centers, which represent triborane analogue (Figure 3c). Further, the HOMO of **3** signifies the delocalized orbitals over one of the Ta-B-Ta bonds and localized p orbital on the Se atom of B-Se bond (Figure 3a). The NBO analysis[23] of **1** and **3** shows that all the boron and tantalum centers have negative natural charges, whereas all the sulfur atoms (for **1**) and selenium atoms (for **3**) have positive natural charges (Table S1). The natural charge analysis and natural valence population analysis of **1** and **3** indicate that the tantalum and boron centers are acting as acceptors, whereas sulfur/selenium atoms are behaving as donors.

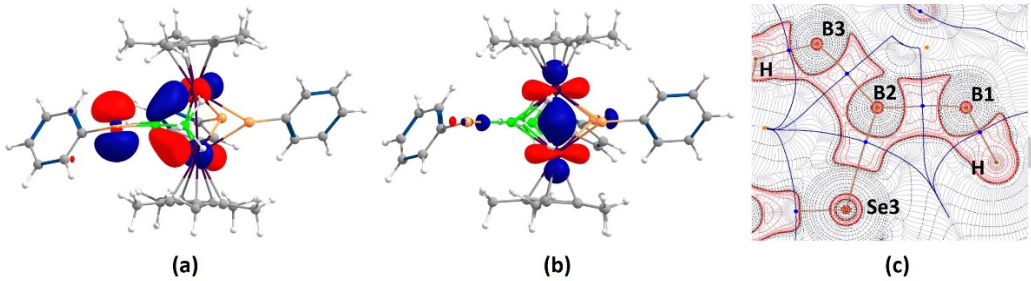

Figure 3. (a) HOMO and (b) HOMO-1 of **3**; (c) Contour line diagram of the Laplacian of electron density of **3** along the B1–B2–B3 plane of **3**.

Tetraborane analogues, 4 and 5. Compounds **4** and **5** were isolated as yellow solids in 20% and 8% yields, respectively. The ^{1}H NMR of **4** and **5** show one Cp* environment at δ = 2.02 and 1.98 ppm, respectively. In addition, compound **4** show three ^{1}H chemical shifts in the negative region at δ = -0.28, -2.03, and -3.04 ppm with 2:2:2 ratio, which may correspond to terminal B-H, bridging B-*H*-B or Ta-*H*-B hydrogens, respectively. In addition, ^{1}H{^{11}B} spectrum of **4** show two chemical shifts at δ = 3.12 and 4.2 ppm, which may correspond to terminal B-H. Whereas compound **5** shows two additional chemical shifts at δ = -0.90, and -2.62 ppm with 2:2 ratio, which correspond to bridging B-*H*-B or Ta-*H*-B hydrogens. The ^{11}B{^{1}H} NMR of **4** and **5** show three resonances at δ = 7.9, 3.3, and -2.8 ppm; and δ = 11.4, 5.0, and -5.2 ppm, respectively with 2:1:1 ratio. The mass spectrum of **4** displays a molecular ion peak at *m/z* 566.1468 [(M-SePh) + CH_3CN]$^{+}$. However, these spectroscopic data were not enough to identify the core geometry of **4** and **5**.

Therefore, we have performed the single-crystal X-ray diffraction analysis on the suitable crystal of **4** and **5**. As presented in Figure 4, the solid-state X-ray analysis reveals compound **4** as [Cp*Ta(SePh)$_2${B_4H_8}] and compound **5** as [Cp*Ta(SePh)$_2${B_4H_7(SePh)}]. Compounds **4** and **5** can be viewed as tetraborane analogues stabilized in the coordination sphere of one tantalum that represent a square pyramidal TaB_4 core, where the tantalum atoms are attached to Cp* and two {SePh} ligands. The only difference between **4** and **5** is the presence of terminal B-SePh in **4**. Both **4** and **5** have 6 SEPs (CVE = 32), however, the square pyramid core needs 7 SEPs for electronic saturation. Thus, compounds **4** and **5** can be viewed as electronically unsaturated species, isoelectronic with earlier reported [Cp*TaCl$_2${B_4H_8}].[7] In **4** and **5**, and [Cp*TaCl$_2${B_4H_8}], the tantalum atoms are at +5 oxidation state. Although there are many examples of tetraborane stabilized in the coordination sphere of two metals,[6,9a] monometal stabilized tetraborane species are very few.

To investigate the effect of substitution of Cl by {SePh} ligand, we have carried out computational analyses of [Cp*TaCl$_2${B_4H_8}], **4**, and **5**. The HOMO-LUMO energy gap for **4** (3.49 eV) and **5** (2.98 eV) are smaller as compared to that of [Cp*TaCl$_2${B_4H_8}] (4.12 eV) (Figure 5). The MO analyses reveal that HOMO of **4** is localized on the Se atom (*p* orbital) of SePh unit attached to the metal center, whereas the HOMO of **5** is centered on the SePh unit attached to boron. On the other hand, the LUMOs of **4** and **5** are mostly centered on tantalum atom (*d*-orbital) along with a little contribution from the Se atom (*p* orbital) of SePh unit attached with the metal center. The NBO analysis shows that the tantalum atom has a negative natural charge in **4** and **5**, and it is positive in [Cp*TaCl$_2${B_4H_8}] (Table S1). This may be due to the higher electronegativity of Cl compared to that of Se. Thus, we believe that the Ta in **4** and **5** acts as an acceptor, whereas it is a donor in [Cp*TaCl$_2${B_4H_8}].

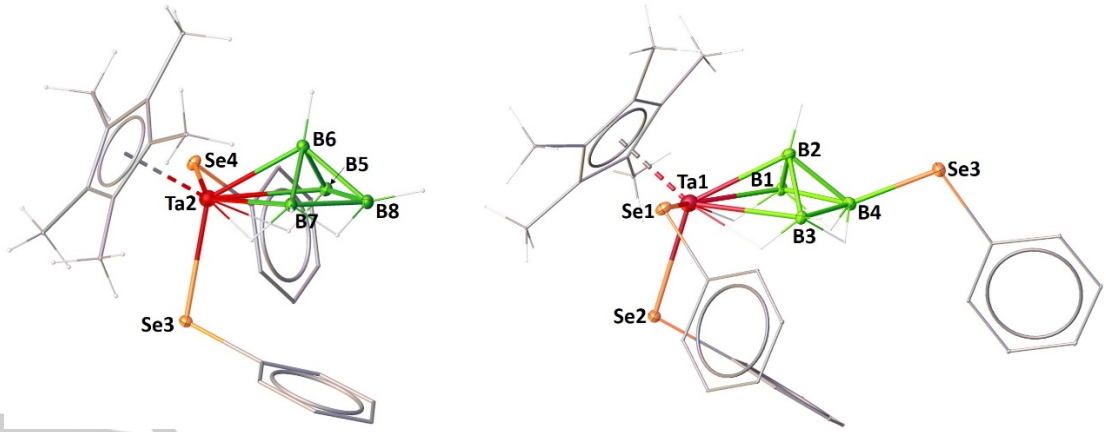

Figure 4. Molecular structure of **4** (left) and **5** (right)**.** Selected bond lengths (Å) and angles (°) of **4**: Ta2-B5 2.47(2), Ta2-B6 2.296(18), Ta2-Se3 2.5870(19), B7-B8 1.84(3), B6-B8 1.75(3); B8-B7-Ta2 98.6(10), B5-Ta2-B7 62.8(7), B5-B8-B7-93.8(13); **5**: Ta1-B1 2.508(11), Ta1-B2 2.277(12), Ta1-Se1 2.5499(11), Ta1-Se2 2.5608(10), B1-B2 1.723(16), B2-B3 1.663(16), B2-B4 1.689(16), B4-Se3 1.969(11); B3-Ta1-B1 63.7(4), B2-B1-B4 57.5(6), B3-B2-B4 64.3(7), B3-B2-B1 102.1(8), B1-B2-Ta1 76.3(6).

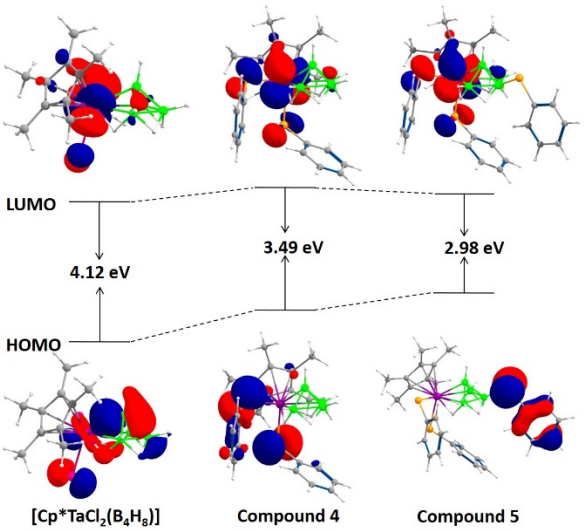

Figure 5. Frontier molecular orbitals of [Cp*TaCl$_2${B$_4$H$_8$}], **4**, and **5**.

Trimetallic polychalcogenide, 2 and 6. Both complexes **2** and **6** were isolated as green solids. The ^{1}H NMR spectrum of **2** shows peaks at δ = 2.24, and 2.11 ppm in 2:1 ratio. On the other hand, the ^{1}H NMR spectrum of **6** shows chemical shifts at δ = 2.34, and 2.24 ppm in 2:1 ratio. The ^{1}H NMR of **2** and **6** reveal the presence of dissimilar Cp* protons, which is further confirmed by ^{13}C{^{1}H} NMR spectra. Although all their spectroscopic data have similar pattern, ^{1}H NMR spectrum of **2** has peaks in the phenyl region. The mass spectra of **2** and **6** show molecular ion peaks at *m/z* 1294.1066 [M]$^+$, and 1502.6188 [M+H]$^+$, respectively. All the spectroscopic data were not adequate to envisage the identity of **2** and **6.** A clear explanation eluded us until the solid-state X-ray structure analysis of **2** and **6** were carried out.

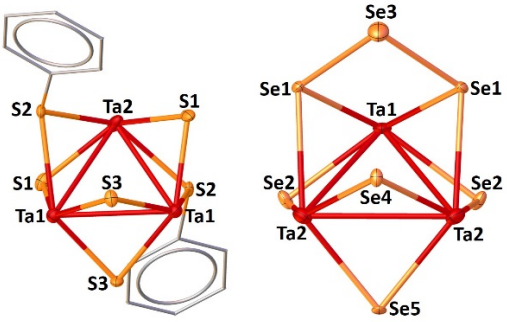

Figure 6. Molecular structure of **2** (left) and **6** (right). Note that Cp* and hydrogens of phenyl groups are not shown for clarity. Selected bond lengths (Å) and angles (°) of **2**: Ta1-Ta1 2.9622(15), Ta1-Ta2 3.2192(12), S1-Ta1 2.427(4), S2-Ta1 2.628(4), S3-Ta1 2.427(4); Ta2-S1-Ta1 84.26(15), Ta2-S2-Ta1 77.24(12); **6**: Ta1-Ta2 3.3311(15), Ta2-Ta2 3.0865(19), Se1-Ta1 2.632(3), Se2-Ta1 2.463(2), Se1-Se3 2.385(4); Se3-Se1-Ta1 95.83(11)

The solid-state X-ray structures of **2** and **6**, shown in Figure 6, show that both the molecules are consist of a Ta$_3$ triangular core that can be viewed as fused trisbutterfly. In the case of **2**, four monosulfide and two {SPh} ligands bridged the edges of the Ta$_3$-triangular framework. Whereas four monoselenide and one triselenide ligand bridged the edges of the triangular Ta$_3$ framework of **6**. One of the interesting features of **6** is the existence of an extra selenide unit above the Ta$_3$Se$_6$ core. This additional selenide unit is not coordinated to any metal, instead bonded to two of the selenium atoms of fused trisbutterfly Ta$_3$Se$_6$ core. Two of the Ta-Ta bond distances in both **2** and **6** differ significantly from the other one. Although the observed Ta1-Ta1 distance of **2** (2.9622(15) Å) and Ta2-Ta2 distance of **6** (3.0865(19) Å) are consistent with normal Ta-Ta bond length, Ta1-Ta2 bond lengths of **2** (3.2192(12) Å) and **6** (3.3311(15) Å) are slightly higher.[19,24] This may be due to the presence of phenyl rings and an additional selenide group in **2** and **6**, respectively.

Table 1. Selected structural parameters of trimetallic polychalcogenide complexes of group 5 metals.

Compounds	*Av.* $d_{M\text{-}M}$ (in Å)[a]	*Av.* $d_{M\text{-}E}$ (in Å) [b]	Ref.
	3.164	2.447	25
	3.262	2.565	24a
	3.232	2.546	24b
	3.133	2.458	This work
	3.249	2.570	This work

[a] *Av.* = Average, [b] E = Chalcogen.

Note that there are few examples of these types of fused trisbutterfly complexes in the literature (Table 1).[24,25] For example, recently utilizing Li[BH$_2$Se$_3$] we have isolated the polychalcogenide trimetallic complexes having Ta$_3$Se$_6$ and Ta$_3$Se$_8$ core. But the earlier attempts to isolate their S analogues utilizing Li[BH$_2$S$_3$] were failed. Now, utilizing phenyl incorporated chalcogenatoborate ligand Li[BH$_3$(SPh)], we are able to isolate

the Ta_3S_6 core (**2**). On the other hand, heptaselenide **6** is the only example of its type after [$Cp^+Nb_3S_7$] ($Cp^+ = C_5Me_4Et$).[25] The MO analysis shows that HOMO-LUMO energy gaps of **2** (2.48 eV**),** and **6** (2.50 eV) are quite higher. Both the HOMOs of **2** and **6** show that d orbitals of each Ta atoms are overlapped with each other and delocalized to form the Ta_3 triangular skeleton (Figures S30a and S30b). Also, we have checked the Laplacian plot of electron density along the Se1-Se3-Se1 plane of **6**, which displayed BCPs and bond path between all these Se atoms (Figure S30c).

UV-vis absorption studies of complexes 1-6. The UV-vis absorption spectroscopy was very helpful to modulate the optical properties of complexes **1-6**. The UV-vis spectra of them reveal multiple bands around 280-700 nm (Fig. 7). The high-energy absorption bands around 280-290 nm point out the π−π* transition of Cp* ligands, and that is characteristic of most of the Cp* based-metal complexes. The low-energy bands around 311-627 nm have been assigned to charge transfer bands.

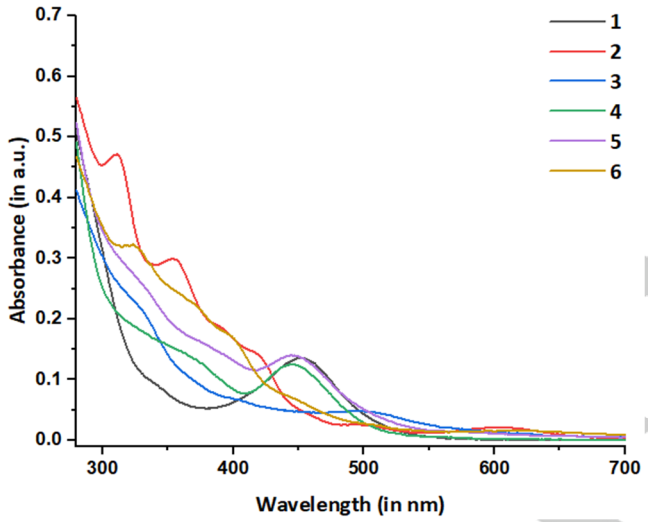

Figure 7. Combined UV-vis spectra of **1-6** in CH_2Cl_2.

In order to get information about the electronic transitions, time-dependent DFT calculations were carried out (Figures S31−S42 and Tables S2−S7). The molecular orbitals related to the most intense electronic transitions of **1-6** are shown in Fig. S37-S42. The absorption bands around 311-420 nm of complexes **1-6** may correspond to the intramolecular MLCT transitions. In complexes **1**, **3**, **4**, and **5**, the absorptions around 445-495 nm may be assigned to the electronic transitions corresponding to HOMO→LUMO. The HOMOs of **1**, **3**, **4**, and **5** are mostly centred on ligands and the LUMOs are localized on d orbitals of Ta with very little contribution from ligand. The absorptions around 445-495 nm, obtained from TD-DFT calculations, may be assigned to intramolecular LMCT transitions. The low-intensity absorptions near 603 and 627 nm for complexes **2** and **6**, respectively, may be due to intramolecular LMCT transitions. They correspond to HOMO-1→LUMO transition in which the HOMO-1 is largely localized on the chalcogen atoms S and Se for complexes **2** and **6**, respectively. Both the LUMOs are centered on the d orbitals of Ta with very little contribution from the ligand.

Conclusion

In summary, we have synthesized and structurally characterized several tantallaheteroborane species, which can be viewed as the result of heteroborane fragment “growth” around a Ta-Ta bond. For example, triborane analogue and diborane analogue are stabilized around the Ta-Ta bond in **1**. In **3**, triborane analogue stabilized around Ta-Ta bond. On the other hand, tetraborane analogues are stabilized in the coordination sphere of Ta. Thus, the isolation and characterization of these unique metallaheteroborane species established a new methodology for the stabilization of diborane, triborane, and tetraborane type species utilizing metal coordination spheres. Further, the theoretical studies revealed that tetraborane species **4** and **5** have reactive Se centers, which can undergo coordination/cluster growth reaction. The reactivity study with metal carbonyls and alkynes is underway.

Experimental Section

General Procedures and Instrumentation. All syntheses were carried out in flame-dried glassware under an argon atmosphere using conventional glovebox or standard schlenk line techniques. Solvents were distilled underneath of Ar atmosphere using standard methods. [Cp*$TaCl_4$][26] and Li[BH_3(EPh)][27,28] (E = S and Se) were synthesized according to the literature methods, while other commercial reagents such as [$LiBH_4$·THF], Ph_2S_2, Ph_2Se_2 powder were used as received (Aldrich) without further purification. The reaction mixture was separated into pure compounds using thin layer chromatographic techniques on 250-µm diameter aluminum supported silica gel TLC plates (MERCK TLC Plates). Note that the reactions, extractions, and work-up were done under Ar-atmosphere, and during all these processes properly distilled solvents were used. In particular, we have done separation using TLC plates inside beakers which were filled with Ar before and after filling with eluting solvents. All the NMR spectra were recorded on Bruker 400 MHz and Bruker 500 MHz FT-NMR spectrometers. ^1H and $^{13}C\{^1H\}$ shifts are referenced to residual ^1H and $^{13}C\{^1H\}$ signals in the deuterated solvent, while $^{11}B\{^1H\}$ resonance is referenced to the external standard of a sealed tube that contained [$Bu_4N(B_3H_8)$] in [D_6] benzene (δ_B = -30.07 ppm).[29] Infrared spectra were recorded on a PerkinElmer Spectrum 400 FT-IR spectrometer. ESI mass spectra were acquired on a Bruker MicroTOF-II mass spectrometer. UV−vis absorption spectra were recorded on a Thermo Scientific (Evolution 300) UV−vis spectrometer. Note that, because of low yields and higher sensitivity, elemental analysis of the compounds could not be performed.

Synthesis of [(Cp*Ta)$_2$(μ-η^3:η^3-B_2H_4S)(μ-η^2:η^2-SBH_3)] (1) and [(Cp*Ta)$_3$(μ-S)$_4$(μ-SPh)$_2$] (2): In a flame-dried 50 mL Schlenk tube under Ar atmosphere, a toluene solution of [Cp*$TaCl_4$] (0.200 g, 0.44 mmol, in 20 mL) was chilled to -78 ºC. Then a freshly prepared toluene solution of Li[BH_3SPh] (4 equivalents, in 15 mL) was transferred to it through a cannula. The reaction mixture was allowed to come to room temperature over 1 hour under the stirring condition and refluxed at 80 °C for 24 h. The solvent was removed in vacuo, and the residue was extracted with n-hexane and filtered through a frit using 3 cm of celite. After removing the solvent from the filtrate, the crude materials were subjected to chromatographic work-up on TLC plates (20% CH_2Cl_2 in hexane) which yielded yellow **1** (0.015 g, 9%) and green **2** (0.019 g, 10%).

1: MS (ESI$^+$): *m/z* calculated for [($C_{20}H_{37}B_3S_2Ta_2$-H) + NH_4]$^+$: 753.1852, found: 753.1644. $^{11}B\{^1H\}$ NMR (160 MHz, [d_8]-toluene, 22 °C): δ (ppm) = 31.8 (br, 1B), -12.0 (br, 1B), -22.6 (br, 1B); ^1H NMR (500 MHz, C_6D_6, 22 °C): δ (ppm) = 6.96 (br, B-H_t), 2.09 (s, 30H; 2×Cp*), -7.99 (d, 2H, Ta-*H*-B), -10.19 (d, 2H, Ta-*H*-B); $^1H\{^{11}B\}$ NMR (500 MHz, [d_8]-toluene, 22 °C): δ (ppm) = 6.81 (s, 1H, B-H_t), 2.08 (s, 30H; 2×Cp*), 0.019 (s, 1H,

B-*H*$_t$), 0.006 (s, 1H, B-*H*$_t$), -8.12 (d, 2H, Ta-*H*-B), -10.30 (d, 2H, Ta-*H*-B); $^{13}C\{^1H\}$ NMR (125 MHz, C_6D_6, 22 °C): δ (ppm) = 110.1 (s, C_5Me_5), 13.6 (s, C_5Me_5); IR (dichloromethane, cm^{-1}): $\tilde{\nu}$ = 2453 (B-*H*$_t$); UV-Vis [CH_2Cl_2, λ, nm]: 343, 451.

2: MS (ESI$^+$): *m/z* calculated for $[(C_{42}H_{55}S_6Ta_3)]^+$: 1294.1068, found: 1294.1066. ^1H NMR (500 MHz, C_6D_6, 22 °C): δ (ppm) = 6.87-6.86 (m, Ph), 2.24 (s, 30H; 2×Cp*), 2.11 (s, 15H; 1×Cp*); $^{13}C\{^1H\}$ NMR (125 MHz, C_6D_6, 22 °C): δ (ppm) = 136.9-126.8 (s, Ph), 119.1, 115.4 (s, C_5Me_5), 13.4, 13.2 (s, C_5Me_5); UV-Vis [CH_2Cl_2, λ, nm]: 311, 353, 420, 494, 603.

Synthesis of [(Cp*Ta)$_2${*μ*-*η*^{3}:*η*^{3}-B$_3$H$_6$(SePh)}{*μ*-SePh}$_2$] (3), [Cp*Ta(SePh)$_2${B$_4$H$_{8-n}$(SePh)$_n$}] (4: n = 0, 5: n = 1), and [(Cp*Ta)$_3$(*μ*-Se)$_4${*μ*-Se$_2$(Se)}] (6): In a flame-dried 50 mL Schlenk tube under Ar atmosphere, a toluene solution of [Cp*TaCl$_4$] (0.200 g, 0.44 mmol, in 20 mL) was chilled to -78 ºC. Then a freshly prepared toluene solution of Li[BH$_3$SePh] (4 equivalents, in 15 mL) was transferred to it via cannula. The reaction mixture was allowed to come to room temperature over 1 hour under the stirring condition and continued for 24 h. The solvent was removed in vacuo, and the residue was extracted with n-hexane and filtered through 3 cm of celite. After removal of the solvent from the filtrate, the crude materials were subjected to chromatographic work-up on TLC plates (20% CH_2Cl_2 in hexane which yielded purple **3** (0.030 g, 12%), yellow **4** (0.059 g, 20%), yellow **5** (0.029 g, 8%), and green **6** (0.022 g, 10%).

3: MS (ESI$^+$): *m/z* calculated for $[C_{38}H_{51}Ta_2B_3Se_3]^+$: 1140.0771, found: 1140.0769. $^{11}B\{^1H\}$ NMR (160 MHz, $CDCl_3$, 22 °C): δ (ppm) = 24.5 (br, 1B), 17.2 (br, 1B), 11.3 (br, 1B); ^1H NMR (500 MHz, C_6D_6, 22 °C): δ (ppm) = 7.96-6.98 (m, Ph), 2.20 (s, 30H; 2×Cp*), -7.00 (s, 2H, Ta-*H*-B), -7.76 (s, 2H, Ta-*H*-B); $^1H\{^{11}B\}$ NMR (500 MHz, C_6D_6, 22 °C): δ (ppm) = 7.53-7.09 (m, Ph), 6.38 (t, 1H, B-*H*$_t$), 6.07 (t, 1H, B-*H*$_t$), 2.28 (s, 30H; 2×Cp*), -7.24 (s, 2H, Ta-*H*-B), -8.09 (s, 2H, Ta-*H*-B); $^{13}C\{^1H\}$ NMR (125 MHz, C_6D_6, 22 °C): δ (ppm) = 137.4-125.7 (s, Ph), 110.5 (s, C_5Me_5), 13.9 (s, C_5Me_5); IR (dichloromethane, cm^{-1}): $\tilde{\nu}$ = 2448 (B-*H*$_t$); UV-Vis [CH_2Cl_2, λ, nm]: 335, 495.

4: MS (ESI$^+$): *m/z* calculated for $[(C_{22}H_{33}TaB_4Se_2$ - SePh) + $CH_3CN]^+$: 566.1491, found: 566.1468. $^{11}B\{^1H\}$ NMR (160 MHz, C_6D_6, 22 °C): δ (ppm) = 7.9 (br, 1B), 3.3 (br, 1B), -2.8 (br, 2B); ^1H NMR (500 MHz, C_6D_6, 22 °C): δ (ppm) = 7.99-6.85 (m, Ph), 4.37 (br, B-*H*$_t$), 3.13 (br, B-*H*$_t$), 2.02 (s, 15H; 1×Cp*), -0.28 (s, 2H, B-*H*$_t$), -2.03 (s, 2H, B-*H*-B), -3.04 (s, 2H, Ta-*H*-B); $^1H\{^{11}B\}$ NMR (500 MHz, C_6D_6, 22 °C): δ (ppm) = 7.98-6.85 (m, Ph), 4.20 (s, 1H, B-*H*$_t$), 3.12 (s, 1H, B-*H*$_t$), 2.02 (s, 15H; 1×Cp*), -0.28 (s, 2H, B-*H*$_t$), -2.03 (s, 2H, B-*H*-B), -3.04 (s, 2H, Ta-*H*-B); $^{13}C\{^1H\}$ NMR (125 MHz, C_6D_6, 22 °C): δ (ppm) = 131.8-127.9 (s, Ph), 118.1 (s, C_5Me_5), 12.5 (s, C_5Me_5); IR (dichloromethane, cm^{-1}): $\tilde{\nu}$ = 2548, 2442 (B-*H*$_t$); UV-Vis [CH_2Cl_2, λ, nm]: 372, 495.

5: $^{11}B\{^1H\}$ NMR (160 MHz, $CDCl_3$, 22 °C): δ (ppm) = 11.4 (br, 2B), 5.0 (br, 1B), -5.2 (br, 1B); ^1H NMR (500 MHz, C_6D_6, 22 °C): δ (ppm) = 7.92-6.87 (m, Ph), 3.59 (br, B-*H*$_t$), 3.49 (s, B-*H*$_t$), 1.98 (s, 15H; 1×Cp*), -0.90 (s, 2H, B-*H*-B), -2.62 (s, 2H, Ta-*H*-B); $^{13}C\{^1H\}$ NMR (125 MHz, C_6D_6, 22 °C): δ (ppm) = 137.6-125.4 (s, Ph), 118.3 (s, C_5Me_5), 12.2 (s, C_5Me_5); IR (dichloromethane, cm^{-1}): $\tilde{\nu}$ = 2545, 2440 (B-*H*$_t$); UV-Vis [CH_2Cl_2, λ, nm]: 381, 445.

6: MS (ESI$^+$): *m/z* calculated for $[(C_{30}H_{45}Se_7Ta_3)$ + H]$^+$: 1502.6247, found: 1502.6188. ^1H NMR (500 MHz, C_6D_6, 22 °C): δ (ppm) = 2.34 (s, 30H; 2×Cp*), 2.24 (s, 15H; 1×Cp*); $^{13}C\{^1H\}$ NMR (125 MHz, C_6D_6, 22 °C): δ (ppm) = 117.1, 114.3 (s, C_5Me_5), 14.9, 14.6 (s, C_5Me_5); UV-Vis [CH_2Cl_2, λ, nm]: 325, 374, 400, 627.

X-ray Structure Determination. Crystal data for **1** was obtained using Bruker AXS Kappa APEX-II CCD diffractometer with graphite-monochromated MoKα (λ = 0.71073 Å) radiation at 150 K. The crystal data for **2**, and **4-6** were collected and integrated Bruker AXS Kappa APEX-III CCD diffractometer with graphite-monochromated MoKα (λ = 0.71073 Å) radiation at 296 K. The crystal data for **3** was collected and integrated using a D8 VENTURE Bruker AXS diffractometer with graphite-monochromated MoKα (λ = 0.71073 Å) radiation at 150 K. The structures were solved by heavy atom methods using SHELXS-97 or SIR92[30] and refined using SHELXL-2018.[31] Olex2 is utilized to draw the structures.[32] Crystallographic data have been deposited with the Cambridge Crystallographic Data Center as supplementary publication no. 2008774 (**1**), 2082990 (**2**), 1914732 (**3**), 2083518 (**4**), 2045971 (**5**), and 2082991 (**6**). These data can be obtained free of charge via www.ccdc.cam.ac.uk/data_request/cif.

1: $C_{20}H_{37}B_3S_2Ta_2$, M_r = 735.94, triclinic, space group *P-1*, *a* = 9.4502(9) Å, *b* =11.3156(10) Å, *c* = 12.0193(12) Å, *α* = 71.843(3)°, *β* = 88.776(4)°, *γ* = 85.061(3)°, *V* = 1216.7(2) Å^3, *Z* = 2, ρ_{calc} = 2.009 g/cm3, *μ* = 9.162 mm^{-1}, *F*(000) = 700.0, R_1 = 0.0275, wR_2 = 0.0563, 5527 independent reflections [2θ ≤ 54.968°] and 564 parameters.

2: $C_{43}H_{57}Cl_2S_6Ta_3$, M_r = 1379.99, tetragonal, space group *P4$_2$/n*, *a* = 12.0855(16) Å, *b* =12.0855(16) Å, *c* = 30.920(4) Å, *α* = *β* = *γ* = 90°, *V* = 4516.2(13) Å^3, *Z* = 4, ρ_{calc} = 2.030 g/cm3, *μ* = 7.677 mm^{-1}, *F*(000) = 2656.0, R_1 = 0.0768, wR_2 = 0.1761, 3987 independent reflections [2θ ≤ 49.990°] and 315 parameters.

3: $C_{38}H_{49}B_3Se_3Ta_2$, M_r = 1136.98, monoclinic, space group *P2$_1$/c*, *a* = 20.0953(16) Å, *b* = 9.9318(7) Å, *c* = 19.6758(16), *α* = 90°, *β* = 105.574(3), *γ* = 90°, *V* = 3782.8(5)Å^3, *Z* = 4, ρ_{calc} =1.996 g/cm^3, *μ* = 8.694mm^{-1}, *F*(000) = 2160.0, R_1= 0.0364, wR_2 = 0.0809, 8651 independent reflections [2θ ≤ 55.014°] and 311parameters

4: $C_{22}H_{33}B_4Se_2Ta$, M_r = 679.59, monoclinic, space group *P2$_1$/c*, *a* = 9.7935(15) Å, *b* = 18.224(3) Å, *c* = 28.933(6) Å, *α* = 90.000(5)°, *β* = 90.02(2)°, *γ* = 90°, *V* = 5163.9(16) Å^3, *Z* = 8, ρ_{calc} = 1.748 g/cm^3, *μ* = 7.083 mm^{-1}, *F*(000) = 2608.0, R_1 = 0.0525, wR_2 = 0.0914, 9094 independent reflections [2θ ≤ 50.074°] and 677 parameters

5: $C_{28}H_{37}B_4Se_3Ta$, M_r = 834.64, orthorhombic, space group *Pbca*, *a* = 20.3246(13) Å, *b* = 14.8799(8) Å, *c* = 20.6315(13) Å, *α* = *β* = *γ* = 90°, *V* = 6239.5(7) Å^3, *Z* = 8, ρ_{calc} = 1.777 g/cm^3, *μ* = 7.039 mm^{-1}, *F*(000) = 3200.0, R_1 = 0.0392, wR_2 = 0.0650, 5493 independent reflections [2θ ≤ 49.998°] and 353 parameters.

6: $C_{31.30}H_{47.60}Cl_{2.60}Se_7Ta_3$, M_r = 1611.42, orthorhombic, space group *Pnma*, *a* = 16.827(2) Å, *b* = 16.111(2) Å, *c* = 15.2247(19) Å, *α* = *β* = *γ* = 90°, *V* = 4127.6(9) Å^3, *Z* = 4, ρ_{calc} = 2.593 g/cm^3, *μ* = 14.296 mm^{-1}, *F*(000) = 2946.0, R_1 = 0.0828, wR_2 = 0.1579, 3764 independent reflections [2θ ≤ 49.998°] and 252 parameters.

Computational Details. All molecules were fully optimized using b3lyp functional[33] in conjunction with the 6-31g(d)-sdd basis set using the Gaussian 09[34] program. For the optimization of all molecules, multiplicity = 1 is considered. All compounds were fully optimized in gaseous state using their X-ray crystallographic coordinates. NBO analyses were carried out with the NBO partitioning scheme[24] as employed in the Gaussian 09. Note that significant algorithmic differences between NBO3 and NBO5 are particularly apparent in details of natural population analysis for transition metals and rare-earth species.[35] Wiberg bond indexes (WBI)[22] were obtained on NBO analysis. The QTAIM analysis[23] was performed utilizing Multiwfn V.3.6 package.[36] The ^{11}B NMR chemical shifts were calculated with respect to B_2H_6 (B3LYP B shielding constant 93.5 ppm) and converted to the usual [$BF_3.OEt_2$] scale using the experimental ^{11}B chemical shift of B_2H_6, 16.6 ppm. All the optimized structures and orbital graphics were produced using the Gaussview[37] and Chemcraft[38].

Acknowledgements

This work was funded by SERB, New Delhi, India, Grant No. CRG/2019/001280. S.K. and S.B. thank IIT Madras and K.K. thank DST-INSPIRE for fellowships. We thank P. K. Sudhadevi Antharjanam and Dr. B. Varghese for X−ray structure analyses. The computational facility, IIT Madras is gratefully acknowledged.

Keywords: Chalcogen • Metallaheteroborane • Tantalum • Tetraborane • Triborane

[1] a) H.-J. Himmel, *Angew. Chem. Int. Ed.* **2019**, *58*, 11600−11617; b) H. Braunschweig, R. D. Dewhurst, *Angew. Chem. Int. Ed.* **2013**, *52*, 3574–3583; c) M. Arrowsmith, H. Braunschweig, T. E. Stennett, *Angew. Chem. Int. Ed.* **2017**, *56*, 96–115.

[2] a) E. C. Neeve, S. J. Geier, I. A. I. Mkhalid, S. A. Westcott, T. B. Marder, *Chem. Rev.* **2016**, *116*, 9091−9161; b) T. Trageser, M. Bolte, H.-W Lerner, M. Wagner, *Angew. Chem. Int. Ed.* **2020**, *59*, 7726–7731; c) L. Kong, W. Lu, Y. Li, R. Ganguly, R. Kinjo, *J. Am. Chem. Soc.* **2016**, *138*, 8623–8629. d) A. Widera, E. Filbeck, H.-J Himmel, *Eur. J. Inorg. Chem.* **2020**, 3017–3029.

[3] E. Osorio, J. K. Olson, W. Tiznado, A. I. Boldyrev, *Chem. Eur. J.* **2012**, *18*, 9677–9681.

[4] S. Aldridge, M. Shang, T. P. Fehlner, *J. Am. Chem. Soc.* **1998**, *120*, 2586–2598.

[5] a) A. DiPasquale, X. Lei, T. P. Fehlner, *Organometallics* **2001**, *20*, 5044–5049; b) X. Lei, M. Shang, T. P. Fehlner, *J. Am. Chem. Soc.* **1999**, *121*, 1275–1287; c) Y. Nishihara, K. J. Deck, M. Shang, T. P. Fehlner, B. S. Haggerty, A. L. Rheingold, *Organometallics* **1994**, *13*, 4510–4522.

[6] (a) S. Ghosh, M. Shang, T. P. Fehlner, *J. Organomet. Chem.* **2000**, *614−615*, 92−98; b) K. J. Deck, Y. Nishihara, M. Shang, T.P. Fehlner, *J. Am. Chem. Soc.* **1994**, *116*, 8408−8409; c) J. Ho, K. J. Deck, Y. Nishihara, M. Shang, T. P. Fehlner, *J. Am. Chem. Soc.* **1995**, *117*, 10292−10299; d) S. K. Bose, K. Geetharani, B. Varghese, S. M. Mobin, S. Ghosh, *Chem. Eur. J.* **2008**, *14*, 9058−9064.

[7] S. Aldridge, H. Hashimoto, M. Shang, T. P. Fehlner, *Chem. Commun.* **1998**, 207−208.

[8] a) C. Lenczyk, D. K. Roy, K. Oberdorf, J. Nitsch, R. D. Dewhurst, K. Radacki, J.-F. Halet, T. B. Marder, M. Bickelhaupt, H. Braunschweig, *Chem. Eur. J.* **2019**, *25*, 16544–16549; b) H. Braunschweig, Q. Ye, A. Vargas, R. D. Dewhurst, K. Radacki, A. Damme, *Nat. Chem.* **2012**, *4*, 563–567.

[9] a) K. Saha, S. Ghorai, S. Kar, S. Saha, R. Halder, B. Raghavendra, E. D. Jemmis, S. Ghosh, *Angew. Chem. Int. Ed.* **2019**, *58*, 17684−17689; b) B. Mondal, R. Bag, S. Ghorai, K. Bakthavachalam, E. D. Jemmis, S. Ghosh, *Angew. Chem. Int. Ed.* **2018**, *57*, 8079–8083; c) R. Borthakur, K. Saha, S. Kar, S. Ghosh, *Coord. Chem. Rev.* **2019**, *399*, 213021.

[10] a) T. P. Fehlner, *Organometallics* **2000**, *19*, 2643-2651; b) T. P. Fehlner, J.-F. Halet, J.-Y. Saillard, *Molecular Clusters. A Bridge to Solid-State Chemistry*; Cambridge University Press: New York, **2007**.

[11] a) L. Barton, D. K. Srivastava in *Metallaboranes. Comprehensive Organometallic Chemistry II, Vol. 1* (Eds.: E. F. Abel, G. A. Stone, G. Wilkinson), Pergamon: New York, **1995**, pp. 275−372; b) T. P. Fehlner, *Pure Appl. Chem.* **2006**, *78*, 1323–1331; c) K. Geetharani, S. Tussupbayev, J. Borowka, M. C. Holthausen, S. Ghosh,. *Chem. Eur. J.* **2012**, *18*, 8482–8489; d) H. Chen, J. F. Hartwig, *Angew. Chem. Int. Ed.* **1999**, *38*, 3391−3393.

[12] R. Hoffmann, *Angew. Chem. Int. Ed. Engl.* **1982**, *21*, 711–724.

[13] a) K. Wade, *J. Chem. Soc. D* **1971**, 792−793; b) K. Wade, *Adv. Inorg. Chem. Radiochem.* **1976**, *18*, 1−66; c) M. A. Fox, K. Wade, *Pure Appl. Chem.* **2003**, *75*, 1315−1323.

[14] D. M. P. Mingos, *Acc. Chem. Res.* **1984**, *17*, 311−319.

[15] E. D. Jemmis, M. M. Balakrishnarajan, P. D. Pancharatna, *Chem. Rev.* **2002**, *102*, 93−144.

[16] M. G. Chowdhury, S. K. Barik, K. Saha, B. Kirubakaran, A. Banerjee, V. Ramkumar, S. Ghosh, *Inorg. Chem.* **2018**, *57*, 985−994.

[17] a) K. K. V. Chakrahari, S. Ghosh, *J. Chem. Sci.* **2011**, *123*, 847−851; b) B. Joseph, S. K. Barik, R. Ramalakshmi, G. Kundu, T. Roisnel, V. Dorcet, S. Ghosh, *Eur. J. Inorg. Chem.* **2018**, 2045–2053; c) S. Sahoo, S. M. Mobin, S. Ghosh, *J. Organomet. Chem.* **2010**, *695*, 945−949.

[18] The calculated ^{11}B chemical shifts of **3** appeared at δ = 23.0, -20.6, and -28.9 ppm.

[19] S. Kar, S. Saha, K. Saha, K. Bakthabachalam, V. Dorcet, S. Ghosh, *Inorg. Chem.* **2018**, *57*, 10896–10905.

[20] C. Ting, L. Messerle, *J. Am. Chem. Soc.* **1989**, *111*, 3449–3450.

[21] K. Wiberg, *Tetrahedron* **1968**, *24*, 1083−1096.

[22] a) R. F. W. Bader, *Atoms in Molecules: A Quantum Theory*; Oxford University Press: Oxford, U. K., **1990**; b) R. F. W. Bader, *J. Phys. Chem. A*. **1998**, *102*, 7314−7323; c) R. F. W. Bader, *Chem. Rev*. **1991**, *91*, 893−928.

[23] a) E. D. Glendening, A. E. Reed, J. E. Carpenter, F. Weinhold, *NBO Program 3.1,* W. T. Madison, **1988**; b) A. E. Reed, F. Weinhold, L. A. Curtiss, *Chem. Rev.* **1988**, *88*, 899−926; c) F. Weinhold, R. Landis, *Valency and bonding:A natural bond orbital donor-acceptor perspective;* Cambridge University Press: Cambridge, U.K, **2005**.

[24] a) S. Kar, S. Bairagi, K. Saha, B. Raghavendra, S. Ghosh, *Dalton Trans.* **2019**, *48*, 4203−4210; b) K. Saha, S. Kar, S Ghosh, *J. Indian Chem. Soc.* **2018**, *95*, 729.

[25] J.-C. Leblanc, C. Moise, F. Volpato, H. Brunner, G. Gehart, J. Wachter, B. Nuber, *J. Organomet. Chem.* **1995**, *485*, 237–242.

[26] Z. J. Tonzetich, R. Eisenberg, *Inorg. Chim. Acta* **2003**, *345*, 340−344.

[27] R. Ramalakshmi, K. Saha, D. K. Roy, B. Varghese, A. K. Phukan; S. Ghosh, *Chem. Eur. J.* **2015**, *21*, 17191.

[28] M. T. Mock, R. G. Potter, D. M. Camaioni, J. Li, W. G. Dougherty, W. S. Kassel, B. Twamley, D. L. DuBois, *J. Am. Chem. Soc.* **2009**, *131*, 14454−14465.

[29] G. E. Ryschkewitsch, K. C. Nainan, *Inorg. Synth.* **1974**, *15*, 113−114.

[30] G. M. Sheldrick, *SHELXS-97*; University of Göttingen: Göttingen, Germany, **1997**.

[31] G. M. Sheldrick, *Acta Crystallogr., Sect. C: Struct. Chem.* **2015**, *71*, 3−8.

[32] O. V. Dolomanov, L. J. Bourhis, R. J. Gildea, J. A. K. Howard, H. J. Puschmann, *Appl. Crystallogr.* **2009**, *42*, 339−341.

[33] a) A. D. Becke, *J. Chem. Phys.* **1993**, *98*, 5648−5652; b) A. D. Becke, *Phys. Rev. A*. **1988**, *38*, 3098−3100. (c) C. Lee, W. Yang, R. G. Parr, *Phys. Rev. B.* **1988**, *37*, 785−789.

[34] M. J. Frisch, G. W. Trucks, H. B. Schlegel, G. E. Scuseria, M. A. Robb, J. R. Cheeseman, G. Scalmani, V. Barone, B. Mennucci, G. A. Petersson, H. Nakatsuji, M. Caricato, X. Li, H. P. Hratchian, A. F. Izmaylov, J. Bloino, G. Zheng, J. L. Sonnenberg, M. Hada, M. Ehara, K. Toyota, R. Fukuda, J. Hasegawa, M. Ishida, T. Nakajima, Y. Honda, O. Kitao, H. Nakai, T. Vreven, J. A. Montgomery Jr., J. E. Peralta, F. Ogliaro, M. Bearpark, J. J. Heyd, E. Brothers, K. N. Kudin, V. N. Staroverov, R. Kobayashi, J. Normand, K. Raghavachari, A. Rendell, J. C. Burant, S. S. Iyengar, J. Tomasi, M. Cossi, N. Rega, J. M. Millam, M. Klene, J. E. Knox, J. B. Cross, V. Bakken, C. Adamo, J. Jaramillo, R. Gomperts, R. E. Stratmann, O. Yazyev, A. J. Austin, R. Cammi, C. Pomelli, J. W. Ochterski, R. L. Martin, K. Morokuma, V. G. Zakrzewski, G. A. Voth, P. Salvador, J. J. Dannenberg, S. Dapprich, A. D. Daniels, Ö. Farkas, J. B. Foresman, J. V. Ortiz, J. Cioslowski, D. J. Fox, *Gaussian 09*, *Revision C.01*, Gaussian, Inc., Wallingford, CT, **2010**.

[35] F. Weinhold, C. E. Landis, *Discovering Chemistry with Natural Bond Orbitals*, John Wiley & Sons, Hoboken, **2012**.

[36] T. Lu, F. Chen, *J. Comput. Chem.* **2012**, *33*, 580−592.

[37] I. I. Dennington, R. T. Keith, J. Millam, K. Eppinnett, W. L. Hovell, R. Gilliland, *GaussView*, *Version 3.09*; Semichem Inc.: Shawnee Mission, KS, **2003**.

[38] G. A. Zhurko, http://www.chemcraftprog.com.

10.1002/ejic.202100687

Entry for the Table of Contents

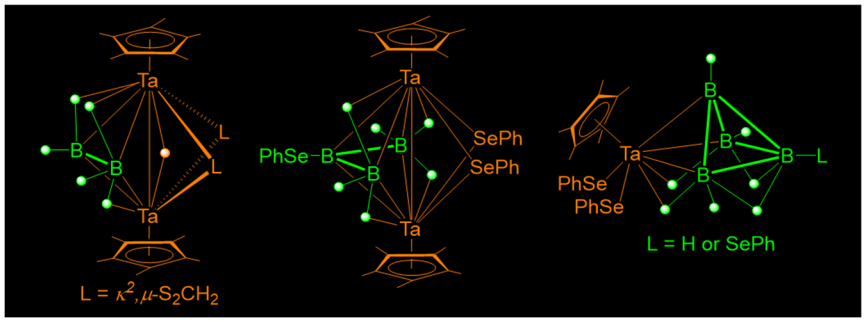

Diborane, triborane analogue, and tetraborane analogue stabilized in the coordination sphere of tantalum atom(s). New early transition metal coordinated triborane and tetraborane analogues have been synthesized utilizing chalcogenatoborate ligands Li[BH_3(EPh)] (E = S or Se) and structurally characterized. Also, theoretical calculations have given insight into their bonding and electronic structures.

Institute and/or researcher Twitter usernames: @GhoshLaB_IITM @kar_sourav @subhashb818 @iitmadras